Eur. Phys. J. A **45**, 287–292 (2010)
DOI 10.1140/epja/i2010-11011-4

THE EUROPEAN PHYSICAL JOURNAL A

Regular Article – Experimental Physics

# Study of collisions of the radioactive $^{24}$Ne beam at 7.9 MeV/u on $^{208}$Pb

G. Benzoni[1,a], F. Azaiez[2], G.I. Stefan[2,3], S. Franchoo[2], S. Battacharyya[3], R. Borcea[4], A. Bracco[1,5], L. Corradi[6], D. Curien[7], G. De France[3], Zs. Dombradi[8], E. Fioretto[6], S. Grevy[3], F. Ibrahim[3], S. Leoni[1,5], D. Montanari[1,5], G. Mukherjee[3], G. Pollarolo[9], N. Redon[10], P.H. Regan[11], C. Schmitt[3,10], G. Sletten[12], D. Sohler[8], M. Stanoiu[2,4], S. Szilner[13], and D. Verney[2]

[1] INFN sezione di Milano, via Celoria 16, I-20133 Milano, Italy
[2] IPN, IN2P3-CNRS, F-91406 Orsay Cedex, France
[3] GANIL, B. P. 55027, F-14076 Caen Cedex 5, France
[4] Horia Hulubei National Institute of Physics and Nuclear Engineering, RO-077125 Bucharest, Romania
[5] Università degli Studi di Milano, via Celoria 16, I-20133 Milano, Italy
[6] INFN-Laboratori Nazionali di Legnaro, viale dell'Università 2, I-35020 Legnaro, Italy
[7] IPHC, IN2P3-CNRS and Universitè Louis Pasteur, 67037 Strasbourg Cedex 2, France
[8] Institute of Nuclear Research of the Hungarian Academy of Sciences, P.O. Box 51, Debrecen, H-4001, Hungary
[9] Dipartimento di fisica Teorica, Università di Torino, and INFN sezione di Torino, I-10125 Torino, Italy
[10] IPNL, IN2P3-CNRS and Université Claude Bernard, 69622 Villeurbanne Cedex, France
[11] Department of Physics, University of Surrey, Guildford, GU2 7XH, UK
[12] Niels Bohr Institute, University of Copenhagen, DK-2100 Copenhagen, Denmark
[13] Ruder Boskovic Institute, HR-10001 Zagreb, Croatia

Received: 18 January 2010 / Revised: 18 June 2010
Published online: 21 July 2010 – 
Communicated by N. Alamanos

**Abstract.** Cross-sections of the main reaction channels for the collision $^{24}$Ne + $^{208}$Pb at 7.9 MeV/u were studied using the radioactive ion beam delivered by the SPIRAL facility and the VAMOS-EXOGAM experimental set-up. Angular distributions for the elastic and inelastic channels were extracted, together with distributions for the +1n and −1p channels. A comprehensive description of the present data is made within the GRAZING model approach.

## 1 Introduction

Multi-nucleon transfer (MNT) and deep inelastic collisions (DIC) with radioactive beams at a few MeV/u are expected to become important tools to reach nuclei further away from stability and study their structure focussing on near-yrast states. These studies are foreseen to become important as a part of the SPIRAL2 radioactive ion beams physics program, in particular around the VAMOS set-up, and with stable beams, around the S3 spectrometer where products from deep inelastic and MNT collisions will be separated and transported onto secondary targets [1].

A wealth of nuclear-structure information is available for MNT and DIC reactions induced by stable beams in several mass regions, particularly for neutron-rich nuclei (see [2] and references therein). Reaction mechanism studies have also been pursued in the last years to study the mass and charge yields, cross-sections and distributions of total kinetic energy loss for multi-neutron and multi-proton transfer channels (see, *e.g.*, ref. [3] and references therein). However, there is a lack of data for medium light projectiles and, moreover, no data exist for reactions induced by radioactive beams. The latter are needed for a comprehensive understanding of the mechanisms underlying these reaction processes. These timely issues have motivated the first measurement with a light radioactive beam, performed employing the reaction $^{24}$Ne + $^{208}$Pb at 7.9 MeV/u.

In transfer reactions induced by neutron-rich projectiles, $Q$-value arguments favour not only the pick-up of neutrons and stripping of protons, but stripping of neutrons and pick-up of protons become available. The identification of these channels, not open for reactions induced by stable beams, represents a first important step for a comparison with theoretical models that use these degrees of freedom as building blocks for the construction of the isotopic distributions of the final products.

Results from this analysis, in terms of elastic and one-particle transfer angular distributions are here reported.

[a] e-mail: giovanna.benzoni@mi.infn.it

This is a very important aspect since the understanding of the processes leading to nuclei far from stability through this type of reactions is highly needed in view of experiments with higher-intensity beams, expected to deliver also relevant nuclear-structure information.

## 2 Experimental details

The experiment was performed using the radioactive $^{24}$Ne beam, delivered by the SPIRAL ISOL facility [4], at a laboratory energy of 7.9 MeV/u, well above the Coulomb barrier. The beam intensity amounted to approximately $1.5 * 10^5$ pps for the entire period of data taking of 6 days. A $^{208}$Pb target with a thickness of 10.9 mg/cm$^2$ was chosen to guarantee a counting rate high enough to obtain spectroscopic information through gamma-decay measurements.

The experimental set-up consisted in the coupling of the VAMOS spectrometer to the EXOGAM array, which allowed the detection of projectile-like ions and $\gamma$-rays in coincidence. The VAMOS spectrometer [5] was positioned close to the grazing angle for this reaction (calculated to be 35° with respect to the beam direction after energy loss at mid target). The $\gamma$-rays emitted by projectile- and target-like reaction products were detected by the EXOGAM array [6], consisting of 11 segmented germanium Clover detectors (9 of which were surrounded by their Compton suppression shields) placed around the target, with a photopeak efficiency of 9% at 1 MeV. The EXOGAM detectors were calibrated in energy using the known transitions of the standard radioactive $\gamma$ sources, $^{60}$Co and $^{152}$Eu. The time between the central-contact discriminator of EXOGAM and the Si wall of VAMOS was recorded, this information allowing to select true coincidences and suppress the background due to random coincidences.

The spectrometer VAMOS consists of two large-aperture quadrupoles, a Wien filter (not used in this experiment) and a magnetic dipole operated in mass-dispersive mode to separate the reaction products according to their momentum to charge state ratio ($p/Q$). The focal-plane detectors of VAMOS consist of two position-sensitive drift chambers, giving the coordinates at the focal plane ($X_{foc}$, $Y_{foc}$, $\theta_{foc}$ and $\phi_{foc}$), an ionization chamber divided into 2 sections providing energy loss information ($\Delta E$), and a wall of 21 silicon detectors for the measurement of the residual energy ($E$) of the transported ions. The time of flight (TOF) of the ions was measured between the silicon detectors and the beam radiofrequency. For additional details on individual detectors see refs. [5,7].

Data reduction included the software reconstruction, on an event-by-event basis, of the trajectory of the ions in the spectrometer providing the coordinates and $\theta$-$\phi$ angles at initial target position. A description of the reconstruction algorithms is given in ref. [7]. The procedure used to construct the mass spectra measured with VAMOS consisted of two steps: first a $\Delta E$-$E$ plot was incremented to select the different elements ($Z$), and secondly the quantities $Q$ (ionic charge state) and $A/Q$ (mass over charge) were reconstructed to identify the different isotopes. $Z$ was deduced from the ionic energy loss, $\Delta E$, while the $A/Q$ ratio was calculated combining the TOF and magnetic rigidity ($B\rho$) measurements. In the reaction under analysis, dealing with rather fast light ions, two ionic charge states were transmitted in the spectrometer, corresponding to fully stripped and hydrogen-like nuclei, the second being at the edge of the acceptance of VAMOS, and therefore partly cut. The population of other charge states is expected to be of the order of few percents and they are not transmitted to the focal plane of the spectrometer. Data from the two charge states were sorted separately and added together at the end.

The use of a large-acceptance spectrometer, such as VAMOS, implies the need to correct experimental data for the non-uniform transmission of the reaction products through the spectrometer. The response function of the VAMOS spectrometer, defined as usual as the number of transmitted particles over the number of incoming particles, has been accurately studied and reported in ref. [8], where the effective solid angle is shown to strongly depend on rigidity. Measured data need, therefore, to be corrected for such dependence on an event-by-event basis, to account for acceptance losses. The dependence on the rigidity ensures the correct treatment of each charge state transmitted into the spectrometer.

As an example, the solid angle covered by the fully stripped Ne isotopes transmitted to the focal plane is shown, as function of the relative rigidity, by the filled area in the three panels on the left of the fig. 1, compared to the total solid angle (full line). From top to bottom we see the acceptance of $^{23}$Ne, $^{24}$Ne and $^{25}$Ne. One can notice that $^{24,25}$Ne nuclei lie in the region of larger acceptance, and, therefore, their distribution is little affected by spectrometer cuts, in contrast with $^{23}$Ne.

## 3 Results

### 3.1 Isotope population

Figure 1 shows in 4 panels the mass distributions measured for this reaction with the present set-up. One observes the population of nuclei with different $Z$, ranging from Na ($Z = 11$, namely one proton pick-up) to $O$ ($Z = 8$, two-proton stripping). The largest yield is concentrated on one-neutron pick-up ($^{25}$Ne) and one-neutron stripping channels ($^{23}$Ne). The mass spectrum of the Ne isotopes detected in VAMOS was obtained requiring a coincidence with a $\gamma$-ray detected in the EXOGAM array in order to suppress most of the contributions from elastic scattering of the beam. In this reaction, involving light nuclei, only $\approx 3$ masses per ionic species are transmitted to the focal plane of the spectrometer.

The spectrometer corrections applied to these data are shown for each nucleus by stars in fig. 1. These corrections are espressed as percentage of the solid angle viewed by each species over the total. The severe acceptance cuts on $^{23}$Ne resulted in the poor statistics registered for this isotope.

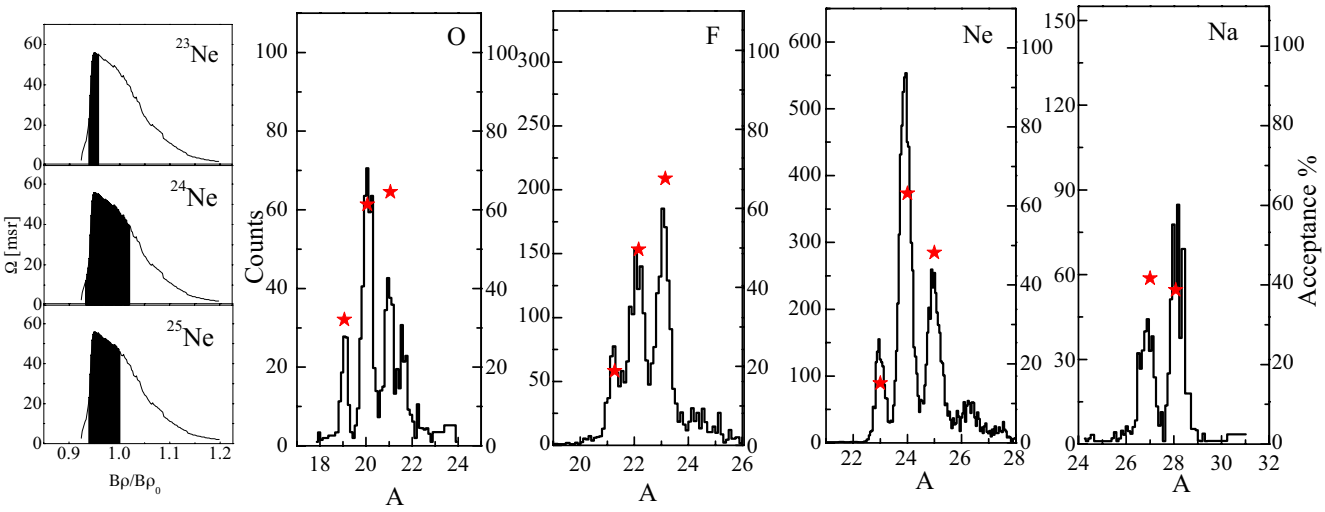


**Fig. 1.** Mass spectra for the different nuclear species populated in the collison $^{24}$Ne (7.9 MeV/u) + $^{208}$Pb are represented in the 4 panels on the right of the spectrum. The spectrum relative to Ne isotopes was sorted with the additional requirement of a coincidence with a $\gamma$-ray to reduce the contribution coming from the pure elastic channel, which dominates the statistics of the 0p0n channel. The solid angle viewed by the three isotopes of Ne (charge state $Q = 10$) is shown by the filled area in the three panels on the left of the figure compared to the total solid angle as a function of the relative rigidity. From top to bottom we see the acceptance of $^{23}$Ne, $^{24}$Ne and $^{25}$Ne. The effective acceptance of each mass, espressed as percentage relative to the total, is reported in each mass spectrum by stars (scale on the right axis of each panel). The experimental mass distributions shown in the figure have been corrected for the spectrometer efficiency, as discussed in the text.

**Table 1.** Measured experimental yields of the detected nuclei reported as percentage relative to the elastic+inelastic channel $^{24}$Ne, compared to GRAZING code predictions. The unit corresponds to a cross-section of $3.5 * 10^4$ mb/sr for the experimental data and $3.6 * 10^4$ mb/sr for GRAZING calculations.

| Nucleus | Channel | Experimental relative yield | GRAZING relative yield |
|---|---|---|---|
| $^{24}$Ne | 0p0n | 100 (0.54) | 100 |
| $^{24}$Ne (inelastic) | | 2.85 (0.09) | |
| $^{23}$Ne | −1n | 0.19 (0.02) | 1.48 |
| $^{25}$Ne | +1n | 3.3 (0.10) | 3.07 |
| $^{23}$F | −1p | 0.65 (0.04) | 0.4 |
| $^{22}$F | −1p-1n | 0.55 (0.04) | 0.003 |
| $^{21}$F | −1p-2n | 0.13 (0.02) | 0.002 |
| $^{21}$O | −2p-1n | 0.16 (0.02) | 0.006 |
| $^{20}$O | −2p-2n | 0.21 (0.03) | 0.006 |
| $^{19}$O | −2p-3n | 0.07 (0.01) | 0.006 |
| $^{27}$Na | +1p+2n | 0.17 (0.02) | $3 * 10^{-4}$ |
| $^{28}$Na | +1p+3n | 0.25 (0.02) | $3 * 10^{-5}$ |

In table 1 the relative yields for the production of the isotopes populated in the present experiment are reported. A sizable population of nuclei such as oxygen and fluorine is seen, being the observation of oxygen isotopes ($^{21,20,19}$O), which correspond to −2p-1n,−2p-2n,−2p-3n channels, of particular relevance. Only two Na isotopes are detected, corresponding to $^{27,28}$Na. In general this is a useful result in view of future exploitation of this reaction mechanism for studies of nuclei far from stability.

The last column of table 1 shows predictions obtanined using the semiclassical code GRAZING [9] integrated over the same angular range accepted by VAMOS in the present configuration. A description of the GRAZING code and a comparison between the results is given in the next section. Both experimental data and predictions are given as yields relative to the elastic+inelastic channel, since this quantity can be directly compared to results from future experiments.

In fig. 2 the $\gamma$-ray spectra measured in coincidence with the most intense channels, $^{24,25}$Ne, are shown in the top and bottom panels, respectively. These spectra have been Doppler corrected on an event-by-event basis thanks to the full reconstruction of the velocity vector deduced using the information from VAMOS. In the inset of each panel the spectra of the corresponding target-like products, $^{208,207}$Pb, are shown. The velocities of the beam-like partners have been calculated assuming a two-body process. The quality of the resulting $\gamma$ spectra confirms both the nucleus identification and the reconstruction of its trajectory into the spectrometer. We would also like to stress the importance of coupling a $\gamma$ array to a spectrometer, in order to certify the mass reconstruction, which is strongly needed in experiments with low statistics.

In the gamma spectrum in coincidence with $^{24}$Ne (upper panel) the peak at 1981 keV corresponds to the $2^+ \rightarrow 0^+$ transition, while the lines at 2614 and 583 kev (inset) are the $3^- \rightarrow 0^+$ and $5^- \rightarrow 3^-$ transitions in $^{208}$Pb. The lower panel shows the gamma spectrum correspond-

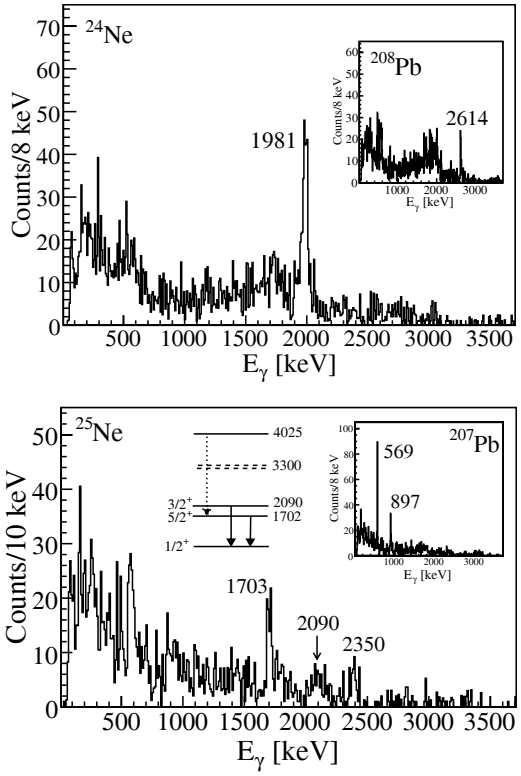


**Fig. 2.** De-excitation spectra of $^{24}$Ne (upper panel) and $^{25}$Ne (lower panel) are shown in the figure, together with the $\gamma$-decay spectra of the corresponding target-like partners ($^{208}$Pb and $^{207}$Pb) in the insets. Main lines are indicated.

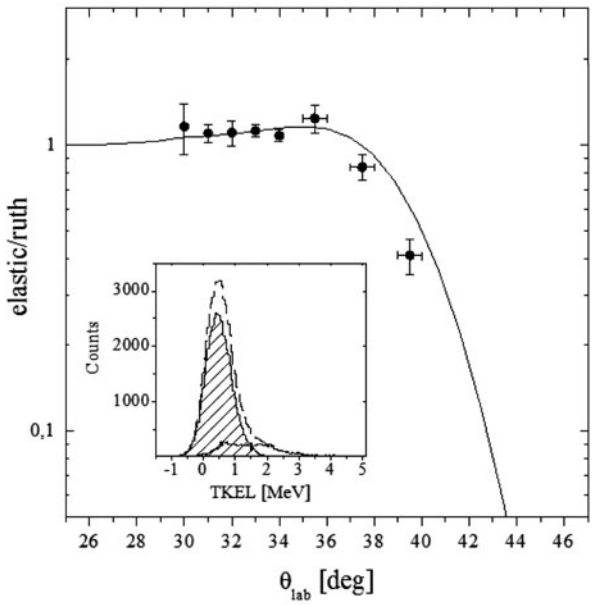


**Fig. 3.** Ratio of the elastic to the Rutherford cross-section over the angular acceptance of VAMOS (full dots) compared to calculations by the GRAZING code (full line). Error bars include statistical and systematic errors of the procedure. In the inset we show the elastic peak (hatched area) obtained by subtracting the $\gamma$-gated TKEL spectrum (full line) from the total TKEL spectrum (dashed line).

ing to $^{25}$Ne and of the associated partner $^{207}$Pb in the inset. In this spectrum one can identify the same transition measured via the neutron transfer (d, p) reaction reported in [10]. In particular the decays from the $5/2^+$ state at 1703 keV and at 2090 keV from the $3/2^+$ state can be recognized. The ordering and the energies of these states have been recently described by new USD calculations by B.A. Brown and W.A. Richter [11]. The $3/2^+$ state is described as a $\nu d_{3/2}$ neutron configuration, while the $5/2^+$ state is described as due to the coupling of the neutron state $\nu s_{1/2}$ to a $2^+$ proton core excitation. A strong peak between 500 and 600 keV is also observed in the spectrum, corresponding to the miscorrected 569 keV peak of the de-excitation of $^{207}$Pb, convoluted with 511 keV annihilation peak. The figure also shows the decay scheme of $^{25}$Ne deduced by the measured transitions. States depicted with dotted lines are either not seen or not confirmed.

### 3.2 Angular distributions

Cross-sections associated to different reaction channels were obtained using the procedure described in [12]. For each scattering angle, two TKEL (total kinetic energy loss) spectra are constructed: the first one is updated with the only requirement of detecting a $^{24}$Ne nucleus in VAMOS (dashed line in the inset of fig. 3), while the second one requiring an additional coincidence with $\gamma$-rays measured by the EXOGAM array (small peak shown with the full drawn line in the inset of fig. 3). To account for the efficiency of the $\gamma$ detection array, these two groups of spectra are normalized in the region above 1.5 MeV, being the first excited state at 1.9 MeV. The normalization factor deduced with this procedure is $\approx 5\%$, consistent with the measured average efficiency of the EXOGAM array for gamma energies greater than 1.5 MeV.

By subtraction, one obtains the spectrum of the elastic component (the peak with a hatched area in the inset of fig. 3). A conversion factor from counts to mbarn is then obtained by setting to 1 the ratio of the measured counts to the Rutherford cross-section in the forward direction, between 31°–33°. In fig. 3 the ratio between the extracted angular distribution to the Rutherford cross-section is shown in comparison with the corresponding calculation obtained by the semiclassical model GRAZING. The agreement gives us confidence on the adopted procedure.

The measured angular distributions associated to the detection of $^{24}$Ne are shown in panel a) of fig. 4. In particular the elastic+inelastic angular distribution is shown with filled circles, the total inelastic is shown with open circles while the inelastic excitation of the first $2^+$ state (1.9 MeV) is shown with filled diamonds. The experimental inclusive (energy integrated) angular distributions for the +1n and −1p channels are shown in panels b) and c) of fig. 4, respectively, in comparison with the prediction obtained by the GRAZING model. The evaluation of angular distributions is limited to few masses owing to the

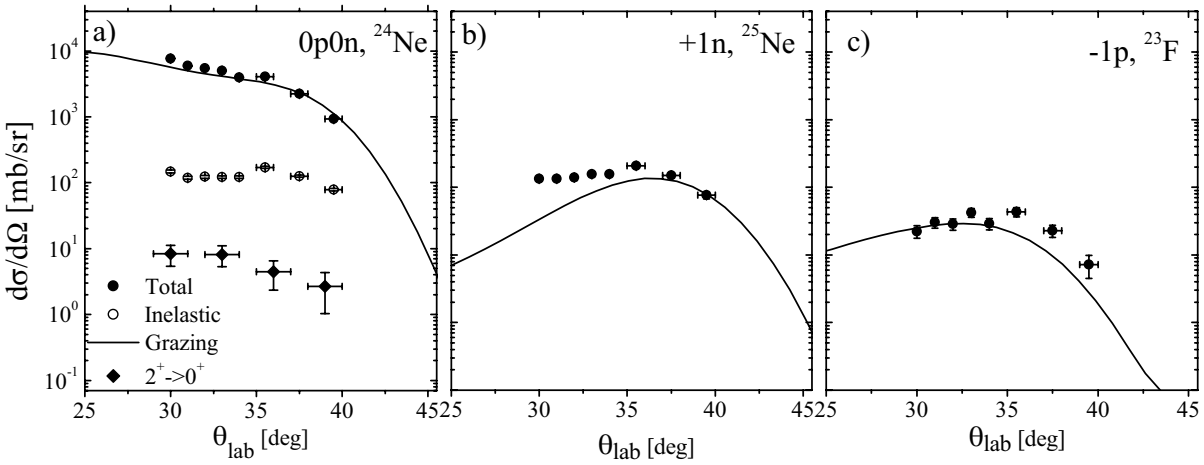


**Fig. 4.** Angular distributions for the most intense channels: 0p0n, +1n, −1p. Data are shown by symbols and calculations by the GRAZING code by full lines. The counts-to-mbarn convertion factor obtained from the comparison shown in fig. 3 has been applied to experimental data. In the case of $^{24}$Ne (panel a)) the figure shows the total angular distribution (full dots), the distribution for the inelastic channels (open dots), obtained by requiring a coincidence with any $\gamma$-ray measured in EXOGAM, and the angular distribution obtained in coincidence with the $2^+ \rightarrow 0^+$ transition at 1.9 MeV (full diamonds). In all panels error bars reflect the statistics and systematic errors.

limited statistics of the dataset. In particular the distribution of $^{23}$Ne is not considered since this nucleus lies at the limits of the acceptance, as described before.

The semiclassical model GRAZING treats the transfer as a sequencial flow of particles, and it is consequently well suited to describe the total cross-sections and angular distributions of channels corresponding to the transfer, both pick-up and stripping, of one particle, while it usually underestimates the transfer of multiple particles, whose description requires the inclusion of more complicated processes.

The agreement between the measurement and the calculation is very good for the elastic+inelastic channel, and reasonably good for the +1n and −1p channels. The discrepancy seen in forward angles for the +1n channel may be related to a contribution from deep inelastic processes that are not taken into account in the theoretical description.

One has to note that this reaction represents an important benchmark case for the GRAZING model itself, which was developed for heavier species and proved to successfully describe reactions that involve the transfer of many nucleons for masses $A > 40$. The drastic change in charge and mass when removing/adding even a single nucleon complicates, in these light nuclei, the description of the reaction mechanism. Moreover at these bombarding energies one expects an interplay between direct reactions and deep inelastic collisions, whose contributions, due to the limited statistics and angular coverage of the present experiment, are difficult to unfold.

In order to have a complete picture of this reaction one would need to measure it on a larger angular range. An increased beam intensity will then allow to study also the weakest channels. The comparison of the same reaction induced by the stable beam $^{22}$Ne will add valuable information on the evolution of this reaction mechanism as a function of $N/Z$.

## 4 Conclusions and perspectives

In summary the present work has provided the first experimental information for a collision induced by a light radioactive beam on a heavy target, at energies around the Coulomb barrier. Angular distributions of a few channels could be studied and found in rather good agreement with predictions from a semiclassical model. Further investigations are needed for a better understanding of the reaction mechanism leading to multiple nucleon transfer. The sizable measured yields point to a future exploitation of this reaction mechanism for studies of nuclear structure in experiments with increased beam intensities.

The authours would like to acknowledge the help and support from the local VAMOS and EXOGAM technical staff for making it possible to run a very smooth experiment, and the GANIL/SPIRAL accelerator crew for providing a particularly stable radioactive $^{24}$Ne beam. The authors would like to acknowledge, in particular, A. Navin and M. Rejmund for their help during both data taking and analysis. This work was partially supported by the EU through the EURONS project under contract No RII3-CT-2004-506065 and by OTKA (Hungary) contract No K68801.

## References

1. M. Lewitowicz, Nucl. Phys. A **805**, 519c (2008).
2. R. Broda, J. Phys. G: Nucl. Part. Phys. **32**, R151 (2006).
3. L. Corradi, G. Pollarolo, S. Szilner, J. Phys. G: Nucl. Part. Phys. **36**, 113101 (2009).
4. A.C.C. Villari, Nucl. Phys. A **693**, 465 (2001).
5. H. Savajols *et al.*, Nucl. Phys. A **654**, 1027c (1999).
6. J. Simpson *et al.*, Acta Phys, Hung., New Ser., Heavy Ion Phys. **11**, 159 (2000).

7. S. Pullanhiotan *et al.*, Nucl. Instrum. Methods Phys. Res. B **266**, 4148 (2008).
8. S. Pullanhiotan *et al.*, Nucl. Instrum. Methods Phys. Res. A **593**, 343 (2008).
9. A. Winther, Nucl. Phys. A **549**, 203 (1995).
10. W.N. Catford *et al.*, Eur. Phys. J. A **25**, S1 250 (2005).
11. B.A. Brown, W.A. Richter, Phys. Rev. C **74**, 034315 (2006).
12. S. Szilner *et al.*, Phys. Rev. C **76**, 024604 (2007).